

A Harmonic Potential Approach for Simultaneous Planning and Control of a Generic UAV Platform

Ahmad A. Masoud

Received: 7 January 2011 / Accepted: 14 April 2011

Abstract Simultaneous planning and control of a large variety of unmanned aerial vehicles (UAVs) is tackled using the harmonic potential field (HPF) approach. A dense reference velocity field generated from the gradient of an HPF is used to regulate the velocity of the UAV concerned in a manner that would propel the UAV to a target point while enforcing the constraints on behavior that were *a priori* encoded in the reference field. The regulation process is carried-out using a novel and simple concept called the: virtual velocity attractor (VVA). The combined effect of the HPF gradient and the VVA is found able to yield an efficient, easy to implement, well-behaved and provably-correct context-sensitive control action that suits a wide variety of UAVs. The approach is developed and basic proofs of correctness are provided along with simulation results.

Keywords Joint planning and control .
Navigation control · Autonomous UAVs ·
Harmonic potential field · Harmonic potential ·
UAV joint planning and control

Nomenclature

P	a point in an abstract N-dimensional space (usually $N = 3$, $P = [x \ y \ z]^t$),
P_s	the starting point,
P_r	the reference or target point,
V	potential field
M	the point mass of the UAV,
F_T	the resultant force along the velocity vector,
F_N	the resultant force normal to the velocity vector,
g	the constant of gravity,
T	the thrust from the UAV engine,
D	the aerodynamic drag,
L	the aerodynamic lift,
K_u, K_λ	are positive constants,
Ω	the workspace,
Γ	boundary of the forbidden regions (obstacles),
Ω'	the region in which directional constraints should be enforced,
$\beta(P)$	a differentiable function that describe in a probabilistic manner everywhere in Ω the fitness of a point P for motion to pass through,
v	the radial speed of the UAV,
γ	flight path angle,
ψ	directional angle,
λ	a vector describing motion in the local coordinates of the UAV, $\lambda = [v \ \gamma \ \psi]^t$,

A. A. Masoud (✉)
Electrical Engineering,
King Fahad University of Petroleum and Minerals,
Dhahran 31261, Saudi Arabia
e-mail: masoud@kfupm.edu.sa

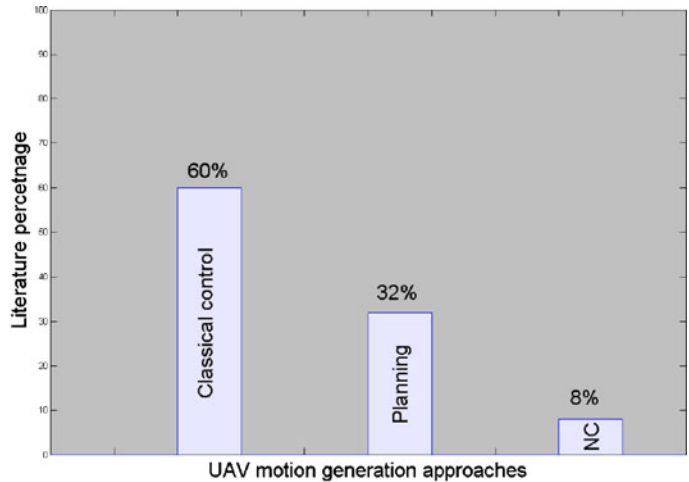
σ	the banking angle,	Ω_s	the set in $P \times \lambda \times u$ where $u \in \Omega_u$
ϵ	the angel of attack,	Γ_s	boundary of Ω_s
$G(\lambda)$	An orthogonal coordinate transformation between the local coordinates of the UAV and its global coordinates,		
$F(\lambda, u)$	the local coordinates state actuation function,		
η_λ	the minimum eigenvalue of Q_λ ($\eta_\lambda > 0$ if the system is fully or redundantly actuated),		
η_P	the minimum eigenvalue of the matrix Q_P ,		
Λ	a vector encoding the directional constraints,		
$\sigma_d(P)$	directionally sensitive fitness measure,		
σ_f	value of σ_d when motion is in accordance with Λ ,		
σ_b	value of σ_d when motion violates Λ ,		
C_L, C_D	positive constants,		
ρ	air density.		
χ	barrier control signal		
$\Xi, \dot{\Xi}$	Liapunov function and its derivative, unconstrained system		
$\Xi_C, \dot{\Xi}_C$	Liapunov function and its derivative, constrained system		
Ω_u	feasible subset of the control space		
Γ_u	boundary of Ω_u		

1 Introduction

The past decade has witnessed a surge in demand for unmanned aerial vehicles (UAVs) to perform critical tasks such as: search and rescue, reconnaissance and target tracking [1–3]. Although the hardware for these robotics agents is becoming commercially available in many different forms (Fig. 1a) at reasonable prices, the software needed to allow reliable, de-skilled operation of these agents is still the focus of intensive study and development [4–6]. It is not uncommon to see form-specific controllers capable of working with only one design while failing to work with others. It is highly unlikely that a controller designed for a fixed-wing UAV [7–9] to work with a helicopter-type [10–12] or a controller designed to work for a helicopter UAV to properly function with a quadrotor UAV [13–15] tilt rotor [16–18] or other types of UAVs [19–21]. This is understandable, since all these agents are severely nonlinear dynamic systems that are subject to nonholonomic constraints making controller design a challenging task.



a: Different types of UAVs,



b: Estimated literature of different approaches for UAV motion generation.

Fig. 1 a Different types of UAVs, b estimated literature of different approaches for UAV motion generation

For these agents to perform a task, a specific type of intelligent, goal/mission-oriented controllers that have the ability to embed the UAV in a given context is needed. These controllers are usually referred to as navigation controllers (NC) or kinodynamic motion planners. Managing the hierarchies of functions needed to support a UAV is being approached by researchers at different levels of the problem with a focus that is limited to individual components of the system or a wider one that aims at integrating more than one essential component in a functioning subsystem of the UAV. Classical controllers that allow a user to direct the UAV along a desired orientation and radial speed were suggested in [22, 23]. A generalization that would allow a UAV to track a target or a reference trajectory was suggested in [24, 25]. Another approach to tackle the problem is to focus only on the kinematic aspects using a planner to translate the context, goal, and mission constraints into a spatial trajectory [26, 27], the existence of a controller that is capable of tracking the trajectory is assumed. The difficult task of joint design of planning and control (navigation control; NC) was attempted with varying degrees of success in [28–30]. Work on the design of modular structures that aim at full system integration may be found in [31, 32].

Despite the intensive effort to develop such controllers and the significant advances achieved there is still a long list of requirements that needs to be addressed. For example almost all of the available controllers are involved, are not easy to tune and require too much processing power. It is desired that the controllers be simple, yet robust, and easy to operate and tune. The controller should also be able to impose a diverse set of constraints in both the workspace of the UAV and in its control space. The ability to integrate, in a provably-correct manner, planning and control is highly desirable if not a must. Due to the high cost of the UAV control software, it is also desirable that the controller accommodate, with minor adjustments, a variety of UAVs.

This paper attempts to jointly address some of the above requirements in a practical manner. It's an extension to the initial results reported in [50]. It develops a flexible, easy to tune, generic navigation controller that is applicable to a wide

range of UAVs. Provably-correct navigation controllers for UAVs are found to be an effective way for the generation of intelligent, context-sensitive, goal-oriented behavior. It is a relatively recent and challenging area that is still in need of a considerable amount of development (Fig. 1b). This type of context-sensitive control is known to have several advantages over the widely used high level-low level context-sensitive control scheme in which a planning stage (high level controller) is connected to a classical controller (low level control). The suggested approach combines an effective and versatile motion planning technique called the harmonic potential field (HPF) motion planner [33, 34], the attractor potential field approach originally suggested by Khatib [35] along with a two-stage model for UAVs. The guidance field from the HPF planner is used to provide the reference velocity field which the UAV must enforce if it is to execute the mission in the desired manner. The attractor field approach along with the two stage model in [43] are combined to work as a virtual velocity attractor (VVA) that would attempt, at an arbitrary point in space, to make the velocity of the UAV coincide with the reference velocity.

2 The HPF Approach: A Background

The harmonic potential field approach is a powerful, versatile and provably-correct means of guiding motion in an N-dimensional abstract space to a goal state subject to a set of constraints that is used to represent an environment. The approach works by converting the goal, representation of the environment and constraints on behavior into a reference velocity vector field (Fig. 2). This reference field is usually generated from a properly conditioned negative gradient of an underlying potential field. A basic setting of the HPF approach is shown below Eq. 1:

$$\begin{aligned} \text{solve : } & \nabla^2 V(P) = 0 \quad P \in \Omega \\ \text{subject to : } & V(P) = 1 \text{ at } P = \Gamma \text{ and } V(P_r) = 0, \end{aligned} \quad (1)$$

A provably-correct path may be generated using the gradient dynamical system:

$$\dot{P} = -\nabla V(P). \quad (2)$$

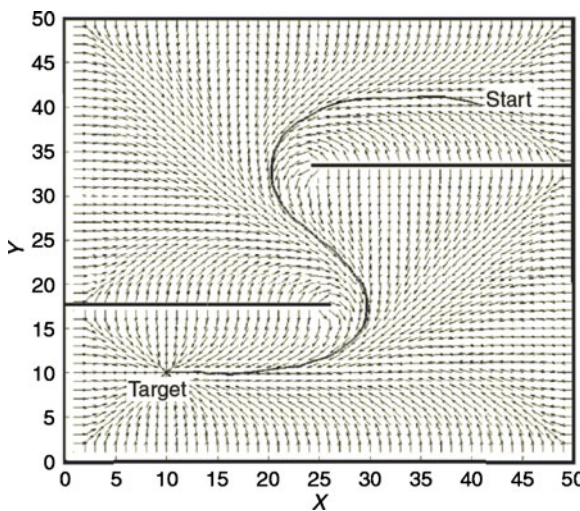


Fig. 2 The reference velocity field from an HPF

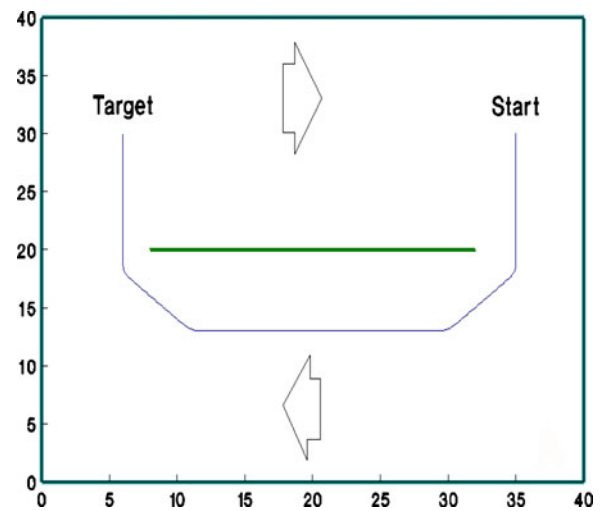


Fig. 4 Directional and regional avoidance constraints

Many variants of the above setting were later proposed to extend the capabilities of the HPF approach. For example, it is demonstrated that the approach can be used for planning in a complex unknown environment [36] relying on local sensing only (Fig. 3),

The HPF approach can incorporate directional constraints along with regional avoidance constraints [37] in a provably-correct manner to plan a path to a target point (Fig. 4). The navigation

potential may be generated using the boundary value problem (BVP):

$$\begin{aligned}
 & \text{jointly solve: } \nabla^2 V(P) \equiv 0 \quad P \in \Omega - \Omega' \\
 & \text{and} \quad \nabla \cdot [\sum(P) V(P)] = 0 \quad P \in \Omega' \\
 & \text{subject to: } V(P) = 1 \text{ at } P = \Gamma \text{ and} \\
 & \qquad \qquad \qquad V(P_r) = 0
 \end{aligned} \tag{3}$$

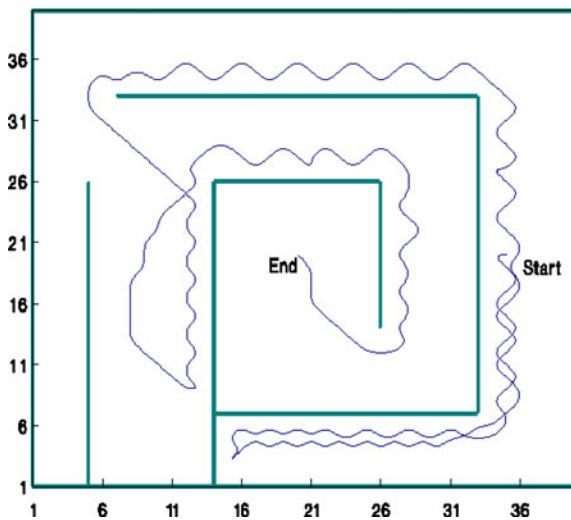
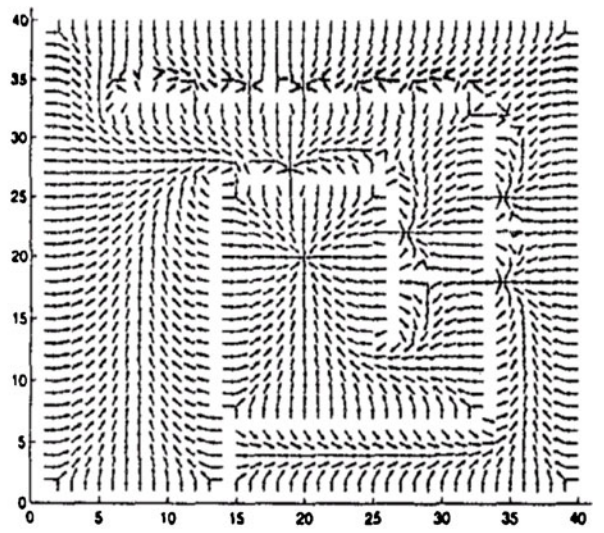


Fig. 3 Planning in unknown environments



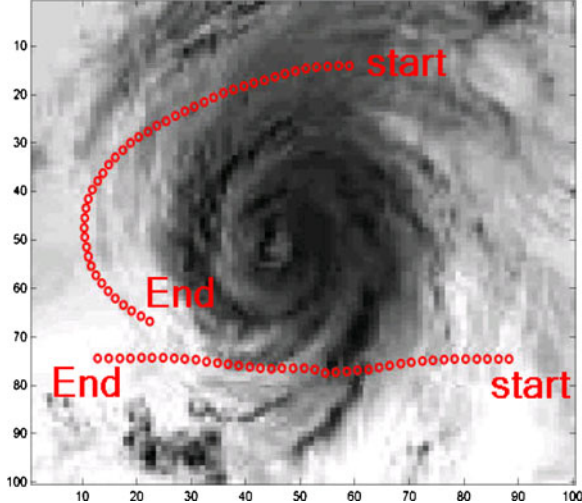


Fig. 5 Planning in non-divisible environments

$$\Sigma(P) = \begin{bmatrix} \sigma(p) & \mathbf{0} & \dots & \mathbf{0} \\ \mathbf{0} & \sigma(p) & \dots & \mathbf{0} \\ \vdots & & & \\ \mathbf{0} & \mathbf{0} & \dots & \sigma(p) \end{bmatrix}$$

where

$$\sigma_d(P) = \begin{bmatrix} \sigma_f - \nabla V(P)^t \Lambda(P) > \mathbf{0} \\ \sigma_b - \nabla V(P)^t \Lambda(P) \leq \mathbf{0} \end{bmatrix}$$

A provably-correct trajectory to the target that enforces both the regional avoidance and directional constraints may be simply obtained using the gradient dynamical system in Eq. 2.

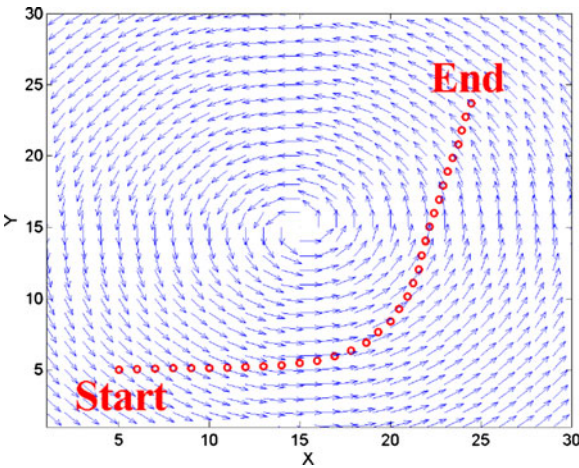


Fig. 6 Planning in the presence of drift fields

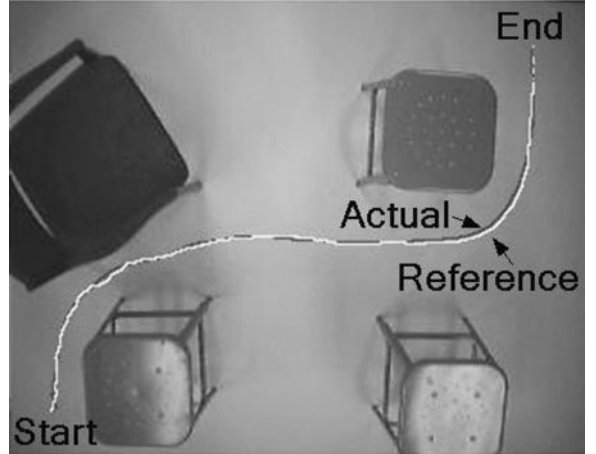


Fig. 7 Integrated, HPF-based navigation

The HPF approach may be modified to take into consideration inherent ambiguity [38] that prevents the partitioning of an environment into admissible and forbidden regions (Fig. 5). The BVP that generates the navigation potential for this case is:

$$\begin{aligned} \text{solve} \quad & \nabla \cdot (\beta(P) \nabla V(P)) = 0 \quad P \in \Omega \\ \text{subject to:} \quad & V(P_s) = 1, \quad V(P_r) = 0 \end{aligned} \quad (4)$$

A provably-correct path that avoids definite threat regions ($\beta(P)=0$) and converge to the target may be generated using the gradient dynamical system in Eq. 2. The HPF-based approach in [38] may be easily modified to take advantage of a drift field that may be present in an environment [39] in a manner that suits planning for energy exhaustive missions (Fig. 6). It was also demonstrated in [40] that the HPF approach can work with integrated navigation systems that can efficiently function in a real-life situation (Fig. 7). Work on extending the HPF approach to work with dynamical and nonholonomic systems may be found in [41–43]. An HPF-based, decentralized, Multi-agent approach was suggested in [47].

3 A Two-Stage Model

A two-stage model to describe motion of a mobile robot was suggested in [43]. The model is based

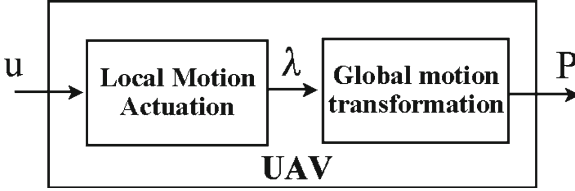


Fig. 8 A two-stage model for UAVs

on dividing a robot into a local actuation stage that couples the control signal to the variables describing the robot's motion in its local coordinates and a global stage that transforms the local variables into world-coordinate motion descriptors. The model, coupled with the HPF approach, was shown to be an effective means for planning motion for mobile robots in both the kinematic and kino-dynamic cases. However the work in [43] is based on the assumption that the local motion actuation stage is invertible. In this work it is shown that the above combination can be effectively utilized in the case where the relation between the control (u) variables and the local motion descriptors (λ) is non-invertible (Fig. 8).

A model that suits most (if not all) UAVs have the form:

$$\begin{aligned}\dot{\mathbf{P}} &= \mathbf{G}(\lambda) \\ \dot{\lambda} &= \mathbf{F}(\lambda, \mathbf{u})\end{aligned}\quad (5)$$

It ought to be noticed that the system equations above do apply to other types of robots such as autonomous under water vehicles (AUVs) [44] and spherical robots [45]. A specific form for

Eq. 5 that describe a fixed-wing (Fig. 9) aircraft [46] is:

$$\dot{x} = v \cdot \cos(\gamma) \cos(\psi)$$

$$\dot{y} = v \cdot \cos(\gamma) \sin(\psi)$$

$$\dot{z} = v \cdot \sin(\gamma)$$

$$\dot{v} = \frac{F_T}{M} - g \cdot \sin(\gamma)$$

$$\dot{\gamma} = \frac{F_N \cdot \cos(\sigma)}{M \cdot v} - g \frac{\cos(\gamma)}{v}$$

$$\dot{\psi} = \frac{F_N \cdot \sin(\sigma)}{M \cdot v \cdot \cos(\gamma)}. \quad (6)$$

$$F_T = T \cdot \cos(\epsilon) - D, \quad F_N = T \cdot \sin(\epsilon) + L \quad (7)$$

$$D = \frac{C_D}{2} \rho v^2, \quad L = \frac{C_L}{2} \rho v^2 \quad (8)$$

4 The HPF-VVA Approach

An HPF-based technique guides motion to a target point and orientation in a provably-correct manner that observes a set of *a priori* specified set of constraints by converting the mission data into a dense vector field that covers the workspace of the agent. This reference field provides at each point the reference velocity instruction that the robot needs to abide by in order for the mission to be accomplished. This process is provably-correct for a massless, single integrator, holonomic system. While it may appear that the capabilities of the HPF approach falls way below the minimum needed to handle the dynamic system in Eq. 5, the approach has properties that are adaptable

Fig. 9 A fixed-wing UAV

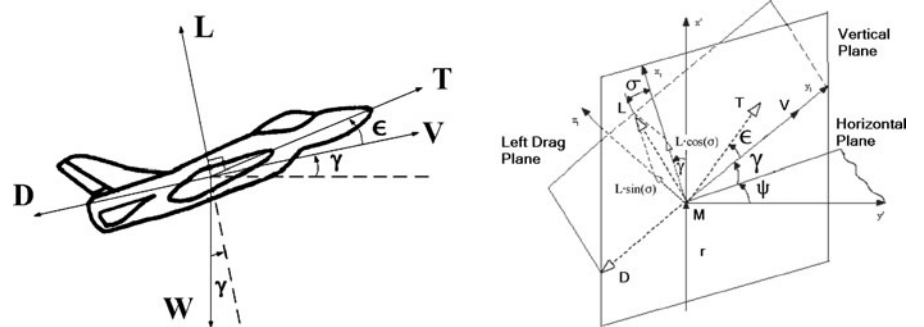
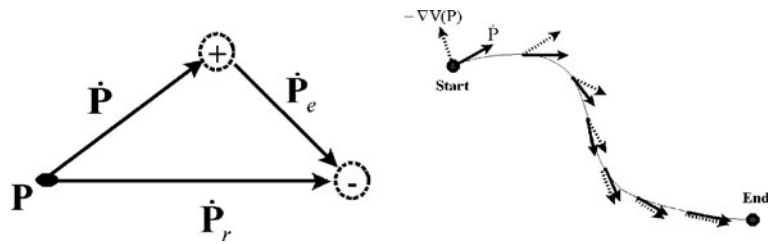


Fig. 10 Linear velocity attractor



for use with severely nonlinear systems such as UAVs. The reference velocity field generated by an HPF method is a region to point planner. In other words successfully executing any guidance instruction irrespective of its location in space will drive the UAV closer to its goal while upholding the constraints. Moreover, the solution trajectories the HPF approach generates are analytic and are expected to be well-behaved when dynamics and nonholonomicity are considered. Therefore if at a point P in space the velocity of the UAV (\dot{P}) is driven to coincide with the velocity reference from the HPF planner ($\dot{P}_r = -\nabla V(P)$), the actual trajectory of the UAV will converge immediately or after a short transient period to the provably-correct trajectory generated by an HPF planner. This may be implemented by constructing an artificial force F_P that attempts to attract the velocity of the UAV to the desired velocity from the HPF planner (Fig. 10)

$$F_P = K_\lambda \cdot (\dot{P}_r - \dot{P}) = K_P \cdot \dot{P}_e. \quad (9)$$

Since the local motion vector λ of the UAV is what causes its velocity in the world coordinate to change ($\dot{P} = G(\lambda)$), a force F_λ in the λ coordinates whose effect is equivalent to F_P has to be constructed using force transformation (Eq. 10):

$$F_\lambda = J_\lambda^T F_P$$

where

$$J_\lambda = \frac{\partial G(\lambda)}{\partial \lambda} \quad (10)$$

The fictitious force F_λ may be used as the desired velocity ($\dot{\lambda}_r = F_\lambda$) in the UAV's local coordinates (λ). In a manner similar to the above, another

artificial force is constructed so that at each point in the coordinates (λ) the local velocity of the UAV ($\dot{\lambda}$) is driven to coincide with the reference velocity $\dot{\lambda}_r$ (Fig. 11). This artificial force (F_u) may be chosen as the scaled error between the two local velocities:

$$\begin{aligned} \dot{\lambda}_e &= \dot{\lambda}_r - \dot{\lambda} \\ F_u &= K_u \cdot \dot{\lambda}_e. \end{aligned} \quad (11)$$

The artificial force in the λ coordinates must be transformed to its equivalent in the control variable coordinates (u). The control coordinate force is used to direct the change of the control signal:

$$\dot{u} = K_u \cdot J_u^T \cdot \dot{\lambda}_e$$

where

$$J_u = \frac{\partial F(\lambda, u)}{\partial u} \quad (12)$$

the control signal fed to the actuators of the UAV may be simply derived as:

$$u(t) = \int_{t_0}^t \dot{u} dt \quad (13)$$

The block diagram of the overall control structure is shown in Fig. 12. The control signal of the

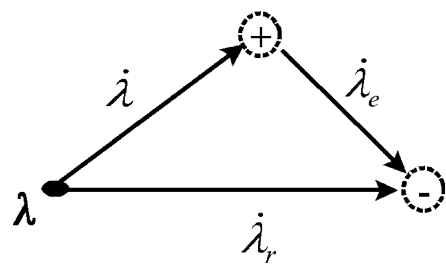


Fig. 11 Local velocity attractor

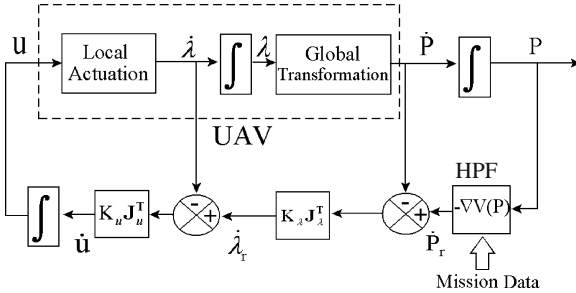


Fig. 12 Suggested navigation control

UAV is generated by jointly solving the nonlinear dynamical systems in Eqs. 5 and 14:

$$\begin{aligned}\dot{u} &= K_u J_u^T [\dot{\lambda}_r - \dot{\lambda}] \\ &= K_u J_u^T [K_\lambda J_\lambda^T (-\nabla V(P) - \dot{P}) - \dot{\lambda}] \\ &= K_u J_u^T [K_\lambda J_\lambda^T (-\nabla V(P) - G(\lambda)) - F(\lambda, u)] \\ &= Q(P, \lambda, u)\end{aligned}\quad (14)$$

As can be seen the VVA approach treats control space in a manner that is similar to workspace where the control signal is viewed as a point moving in space under the influence of a force. This makes it possible to easily apply constraints on the control signal hence jointly constraining state and control spaces. This is achieved by simply augmenting the control signal with a barrier control (χ) to keep u in the feasible part of the control space (Ω_u):

$$\dot{u} = Q(P, \lambda, u) + \chi(u) \quad (15)$$

The simplest and most practical geometry Ω_u may assume is a convex rectangular region of the form:

$$\Omega_u = \{u : u_i^- \leq u_i \leq u_i^+, i=1,..,M\} \quad (16)$$

where u_i^+ and u_i^- are the upper and lower bounds on u_i respectively. The barrier control signal is localized to the boundary of Ω_u ($\Gamma_u = \partial \Omega_u$). The barrier control used with the i 'th component of u (χ_i) may be constructed as:

$$\chi_i(u) = \begin{cases} -K & u_i = u_i^+ \\ +K & u_i = u_i^-, \quad i = 1,..,M \\ 0 & \text{elsewhere} \end{cases} \quad (17)$$

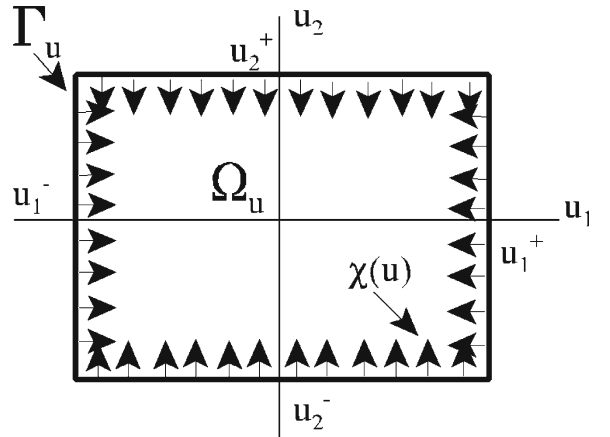


Fig. 13 Barrier control in a 2D control space

where K is a positive constant. The full barrier control may be expressed as the algebraic sum of the individual barrier controls:

$$\chi(u) = \sum_{i=1}^M \chi_i(u_i). \quad (18)$$

In the following section a proof is provided of the ability of the control signal to guarantee stability of the UAV. It is shown that the controller can force the dynamical trajectory of the UAV to mimic the kinematic trajectory from the HPF planner; hence guaranteeing convergence to the target while upholding the constraints encoded in the HPF-generated kinematic trajectory. It is also shown that the dynamic trajectory converges instantly to the kinematic trajectory or, at worst, has an exponential convergence rate which may be directly controlled by K_u and K_λ . The addition of constraints in the control space is proven not to affect convergence where under simple and nonastringent conditions the constrained system is guaranteed to converge to the target point and configuration while maintaining the control signal confined to Ω_u at all time (Fig. 13).

5 Correctness Analysis

This section examines the behavior of the suggested controller.

Proposition 1 The controller suggested in Eq. (14) is unconditionally stable so that for any $K_u >$ and $K_\lambda > 0$:

$$\lim_{t \rightarrow \infty} \dot{P}_e \rightarrow 0. \quad (19)$$

Proof First, the controller is considered to be fast acting so that at a fixed point in space (P) the velocity of the UAV is attracted to a static reference supplied by the negative gradient of the HPF. Proof of the above proposition may be established at two stages: first the error function (Eq. 20) in the local coordinates of the UAV is constructed:

$$E_\lambda(t) = \|\dot{\lambda}_e\|^2 = \|\dot{\lambda}_r - \dot{\lambda}\|^2. \quad (20)$$

Keeping in mind that at a specific point in space, the reference may be considered static, we have:

$$\frac{d}{dt} E_\lambda(t) = -2\dot{\lambda}_e^T \ddot{\lambda}. \quad (21)$$

From Eq. 5 we have:

$$\ddot{\lambda} = \frac{\partial F}{\partial u} \dot{u} \quad (22)$$

$$\frac{d}{dt} E_\lambda(t) = -2\dot{\lambda}_e^T \frac{\partial F}{\partial u} \dot{u} \quad (23)$$

substituting Eq. 14 in Eq. 23, we have:

$$\begin{aligned} \frac{d}{dt} E_\lambda(t) &= -2K_u \dot{\lambda}_e^T \left(\frac{\partial F}{\partial u} \frac{\partial F^T}{\partial u} \right) \dot{\lambda}_e \\ &= -2K_u \dot{\lambda}_e^T Q_\lambda \dot{\lambda}_e \end{aligned} \quad (24)$$

The matrix:

$$\frac{\partial F}{\partial u} \frac{\partial F^T}{\partial u} \geq 0 \quad (25)$$

is at least positive semi-definite. If the rank of the Jacobian matrix is equal to its rows (i.e. the system is fully or redundantly actuated), the matrix in Eq. 25 is positive definite which for this case implies that:

$$\frac{d}{dt} E_\lambda(t) < 0$$

and leads to:

$$\lim_{t \rightarrow \infty} \dot{\lambda}_e \rightarrow 0. \quad (26)$$

In a similar way as above let the following error function be constructed:

$$E_{\dot{P}}(t) = \|\dot{P}_e\|^2 = \|\dot{P}_r - \dot{P}\|^2. \quad (27)$$

$$\frac{d}{dt} E_{\dot{P}}(t) = -2\dot{P}_e \ddot{P}.$$

Since:

$$\ddot{P} = \frac{\partial G}{\partial \lambda} \dot{\lambda} \quad (28)$$

and

$$\lim_{t \rightarrow \infty} \dot{\lambda} \rightarrow \dot{\lambda}_r \quad (29)$$

we have:

$$\ddot{P} = \frac{\partial G}{\partial \lambda} \dot{\lambda}_r = K_P \frac{\partial G^T}{\partial \lambda} \frac{\partial G}{\partial \lambda} \dot{P}_e \quad (30)$$

Therefore:

$$\begin{aligned} \frac{d}{dt} E_{\dot{P}}(t) &= -2K_\lambda \dot{P}_e^T \left(\frac{\partial G^T}{\partial \lambda} \frac{\partial G}{\partial \lambda} \right) \dot{P}_e \\ &= -2K_\lambda \dot{P}_e^T Q_P \dot{P}_e \end{aligned} \quad (31)$$

Since G is an orthogonal coordinate transformation, $(\partial G / \partial \lambda)$ is full rank and the matrix:

$$\frac{\partial G^T}{\partial \lambda} \frac{\partial G}{\partial \lambda} > 0 \quad (32)$$

is positive definite, i.e.

$$\frac{d}{dt} E_{\dot{P}}(t) < 0 \quad (33)$$

is negative definite or equivalently:

$$\lim_{t \rightarrow \infty} \dot{P}_e \rightarrow 0 \quad (34)$$

□

Proposition 2

If $\dot{P}_e(0) = \dot{\lambda}_e(0) = 0$, then $\dot{P}_e(t) = \dot{\lambda}_e(t) = 0 \forall t$. (35)

Proof The $\dot{\lambda}_e$ error measure rate of change may be bounded as:

$$\begin{aligned} \frac{d}{dt} E_{\dot{\lambda}}(t) &= -2K_u \dot{\lambda}_e^T Q_{\lambda} \dot{\lambda}_e \leq -2K_u \eta_{\lambda} \dot{\lambda}_e^T \dot{\lambda}_e \\ &= -2K_u \eta_{\lambda} E_{\dot{\lambda}}(t). \end{aligned} \quad (36)$$

Therefore an upper bound on $E_{\dot{\lambda}}(t)$ may be constructed as:

$$E_{\dot{\lambda}}(t) \leq \exp(-2K_u \eta_{\lambda} t) E_{\dot{\lambda}}(0) \quad (37)$$

As can be seen if $\dot{\lambda}_e(0) = 0$ then $E_{\dot{\lambda}}(0) = 0$. This in turns imply that $E_{\dot{\lambda}}(t) = 0 \forall t$ which leads to $\dot{\lambda}_e(t) = 0 \forall t$. This enables us to bound the error measure rate of change on \dot{P}_e as:

$$\begin{aligned} \frac{d}{dt} E_{\dot{P}}(t) &= -2K_{\lambda} \dot{P}_e^T Q_P \dot{P}_e \leq -2K_{\lambda} \eta_p \dot{P}_e^T \dot{P}_e \\ &= -2K_{\lambda} \eta_p E_{\dot{P}}(t). \end{aligned} \quad (38)$$

As before, the error measure on \dot{P}_e may be bounded as:

$$E_{\dot{P}}(t) \leq \exp(-2K_{\lambda} \eta_p t) E_{\dot{P}}(0) \quad (39)$$

As can be seen if $\dot{P}_e(0) = 0$ then $E_{\dot{P}}(0) = 0$. This implies that $E_{\dot{P}}(t) = 0 \forall t$ which leads to $\dot{P}_e(t) = 0 \forall t$. Even if the initial values of the errors are not equal to zero, the error measures will still exponentially decay with time leading to fast alignment of the velocity vector of the UAV with the reference velocity vector from the gradient of the harmonic potential. □

Proposition 3 let ρ_k be the provably-correct, convergent and constraints-satisfying kinematic trajectory obtained from the gradient of the harmonic potential planner:

$$\rho_k = \{P(t) : \dot{P} = -\nabla V(P)\}. \quad (40)$$

Let ρ_d be the dynamic trajectory of the UAV:

$$\rho_d = \left\{ P(t) : \begin{bmatrix} \dot{P} \\ \dot{\lambda} \\ \dot{u} \end{bmatrix} = \begin{bmatrix} G(\lambda) \\ F(\lambda, u) \\ Q(P, \lambda, u) \end{bmatrix} \right\} \quad (41)$$

if $\dot{P}_e(0) = \dot{\lambda}_e(0) = 0$, then $\rho_d = \rho_k \quad \forall t$.

Proof This result directly follows from Proposition 2. □

Proposition 4 Let

$$u_r = \lim_{t \rightarrow \infty} u(t) \quad (42)$$

resulting from the system:

$$\begin{bmatrix} \dot{P} \\ \dot{\lambda} \\ \dot{u} \end{bmatrix} = \begin{bmatrix} G(\lambda) \\ F(\lambda, u) \\ Q(P, \lambda, u) \end{bmatrix} \quad (43)$$

If

$$u_r \in \Omega_u \quad (44)$$

$$K \geq \max_{P, \lambda, u} |Q(P, \lambda, u)| \quad (45)$$

and u_r is unique at least in Ω_u , then for the system

$$\begin{bmatrix} \dot{P} \\ \dot{\lambda} \\ \dot{u} \end{bmatrix} = \begin{bmatrix} G(\lambda) \\ F(\lambda, u) \\ Q(P, \lambda, u) + \chi(u) \end{bmatrix} \quad (46)$$

we have:

$$\begin{aligned} \lim_{t \rightarrow \infty} P(t) &\rightarrow P_r \\ \lim_{t \rightarrow \infty} \lambda(t) &\rightarrow \lambda_r \\ \lim_{t \rightarrow \infty} u(t) &\rightarrow u_r \end{aligned} \quad (47)$$

and

$$u(t) \in \Omega_u \forall t.$$

Proof Let $R \in P \times \lambda \times u$ and the point $R_T = [P_r \lambda_r u_r]^T$. Since for the unconstrained system we have:

$$\lim_{t \rightarrow \infty} R(t) \rightarrow R_T \quad (48)$$

there exist a Liapunov function $\Xi(R)$ such that:

$$\begin{aligned}\Xi(R) &> 0 \quad \forall R \\ \Xi(R) &= 0 \quad R = R_T\end{aligned}\quad (49)$$

such that: $\dot{\Xi}(R) < 0 \quad \forall R$
 $\dot{\Xi}(R) = 0 \quad R = R_T$

Let Ω_S be an open subset in $R(\Omega_S \subset R)$ such that:

$$\Omega_S = \{R : u \in \Omega_u\} \quad (50)$$

and Γ_s be its boundary ($\Gamma_s = \partial\Omega_S$).

It is not hard to show that if K is selected using Eq. 45, the barrier function will be able to keep u in Ω_u for all t . In other words, R will always be in $\Omega_S \cup \Gamma_s$ for all t . Let $\Xi_c(R)$ be a Liapunov function for the constrained system in Eq. 46, where $\Xi_c(R) = \Xi(R) \forall R \in \Omega_S \cup \Gamma_s$. If $R \in \Omega_S$, i.e. $\chi(u) = 0$, we have:

$$\dot{\Xi}_c(R) = \dot{\Xi}(R). \quad (51)$$

On the other hand, if $R \in \Gamma_s$, then one or more components of the control vector u is kept to a constant value by the barrier control χ . This means that the derivative of $F(\lambda, u)$ with respect to these components is equal to zero. This results in some of the rows of J_u being zeros and could lead to the matrix $J_u^T J_u$ becoming negative semi-definite for the constrained system:

$$\dot{\Xi}_c(R) \leq 0 \quad R \in \Omega_S \cup \Gamma_s. \quad (52)$$

According to the LaSalle invariance principle [49], $R(t)$ will converge to the minimum invariant set. This set may be obtained as the solution of Eq. 53:

$$\begin{bmatrix} G(\lambda) \\ F(\lambda, u) \\ Q(P, \lambda, u) + \chi(u) \end{bmatrix} = 0. \quad (53)$$

By noting that the vector $G(\lambda)$ cannot equal to zero unless the radial velocity v is equal zero, one concludes that it is impossible for the set Γ_s to be a part of the minimum invariant set. This will only leave R_T as the only point in this set. Therefore:

$$\lim_{t \rightarrow \infty} R(t) \rightarrow R_T \quad (54)$$

6 Simulation Results

In this section the capabilities of the suggested navigation control scheme are demonstrated by simulation.

6.1 Fixed Wing UAV

The navigation control is tested for the UAV model in Eq. 4. For this case we have:

$$\begin{aligned}J_\lambda &= \begin{bmatrix} C_\gamma C_\psi & -v \cdot S_\gamma C_\psi & -v \cdot C_\gamma S_\psi \\ C_\gamma C_\psi & -v \cdot S_\gamma C_\psi & v \cdot C_\gamma C_\psi \\ S_\gamma & v \cdot C_\gamma & 0 \end{bmatrix} \\ J_u &= \begin{bmatrix} \frac{1}{M} & 0 & 0 \\ 0 & \frac{C\sigma}{M \cdot v} & \frac{-F_N}{M \cdot v} \cdot S\sigma \\ 0 & \frac{S\sigma}{M \cdot v C_\gamma} & \frac{F_N}{M \cdot v} \cdot \frac{C\sigma}{C_\gamma} \end{bmatrix} \quad (55)\end{aligned}$$

where $C(*) = \cos(*)$, $S(*) = \sin(*)$, $M = 1$, $K_u = 1$, $K_\lambda = 2$.

In the first case the controller is required to fly the UAV at a constant speed ($v_r=1$) along the x direction maintaining $y = z = 2$ starting from the initial position $x = y = z = 0$ and initial configuration $v=0$, $\gamma=0$, $\psi = \pi/4$. Figure 14 shows the spatial trajectory generated by the navigation control and Fig. 15 shows the corresponding x, y, z

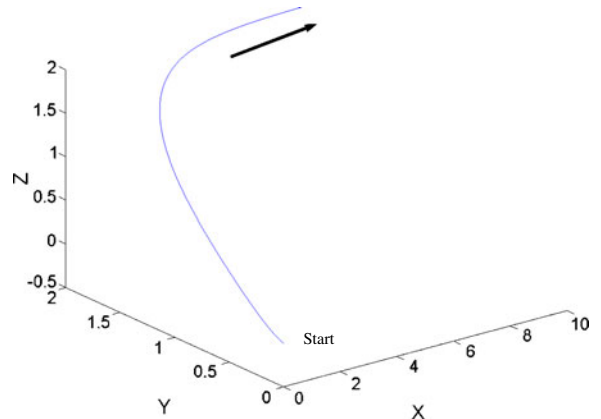


Fig. 14 Spatial trajectory UAV

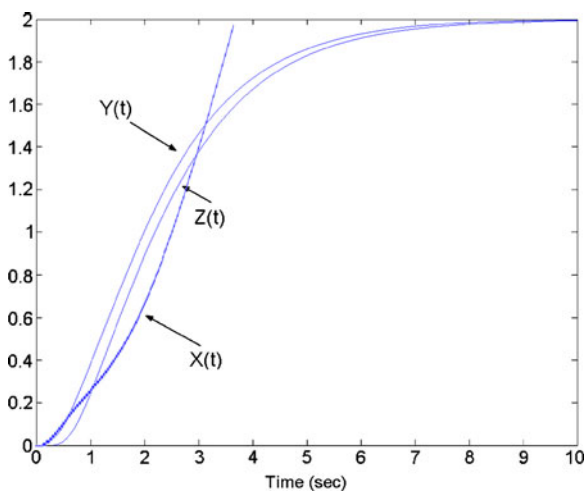


Fig. 15 The xyz components of the trajectory

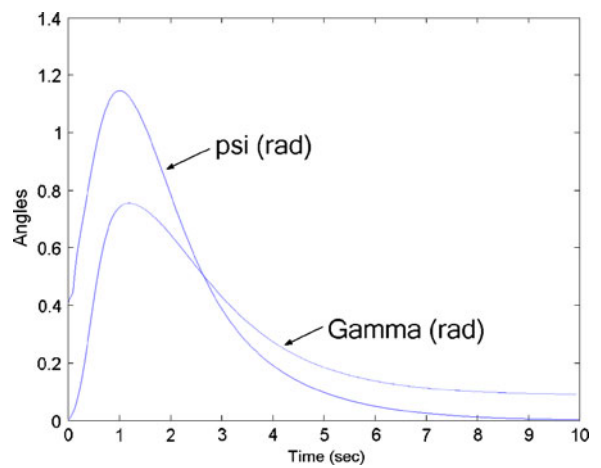


Fig. 17 Orientation of the UAV

of the trajectory versus time. As can be seen, the trajectory is smooth and well-behaved. The radial velocity of the UAV (Fig. 16) quickly settles in a well-behaved manner to the desired radial speed. The orientation angles of the UAV (γ, ψ) as a function of time have a smooth well-behaved profile (Fig. 17). The control variables: banking angle (σ), normal force (F_N) and resultant force along v (F_T) are shown in Figs. 18, 19 and 20 respectively. As can be seen the control signals are bounded and well-behaved.

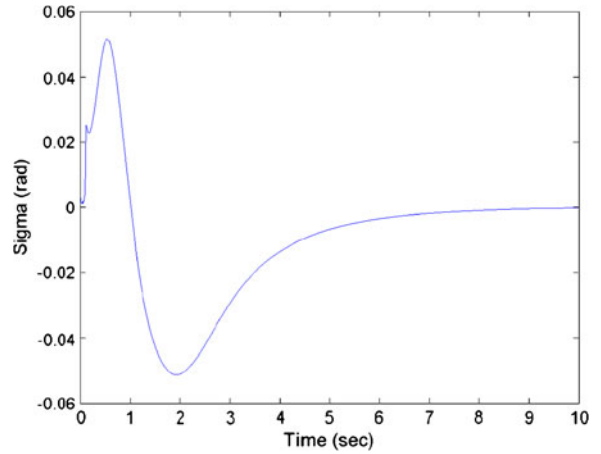


Fig. 18 Banking angle

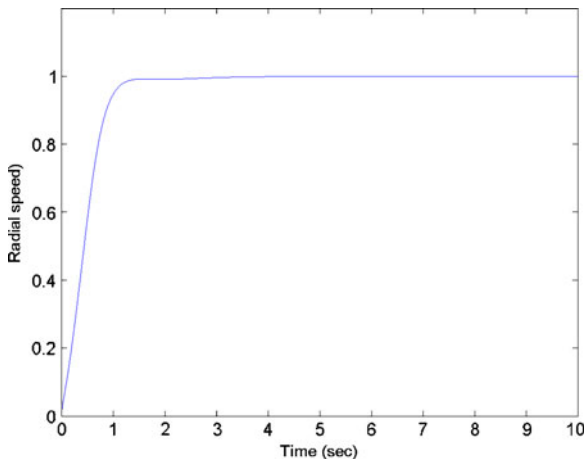


Fig. 16 Radial speed of the UAV

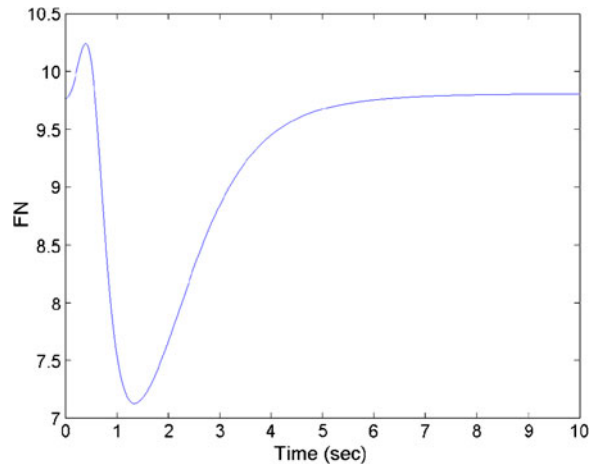


Fig. 19 Normal force

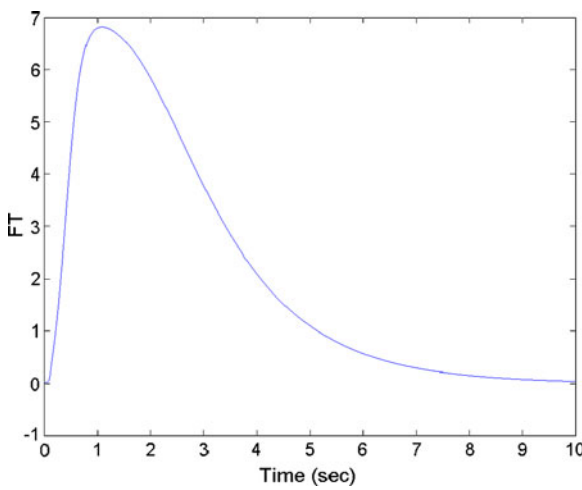


Fig. 20 Tangent force

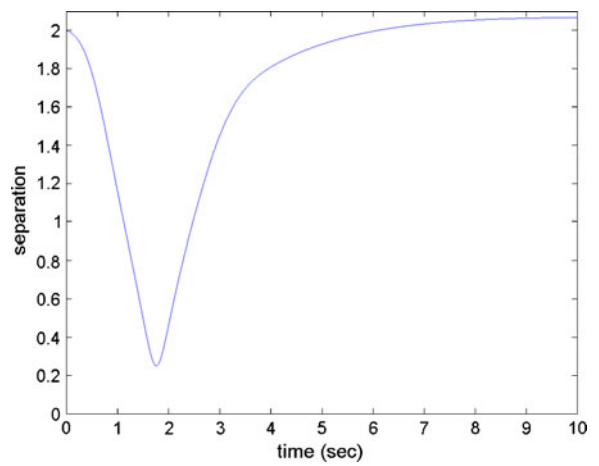


Fig. 22 Distance between the UAVs

In Fig. 21 the control is tested for the multi-UAV case. An antipodal configuration is used to set the UAVs on a potential collision course. Both UAVs are equipped with the suggested navigation control. One UAV is non-cooperative and is treated by the other as an obstacle. As can be seen from the inter-distance curve (Fig. 22), collision was avoided and each UAV proceeded safely towards its destination. The radial speeds of both UAVs are shown in Figs. 23 and 24. It is worth noting that the radial velocity of the maneuvering UAV remained around the rated velocity during the evasion maneuver.

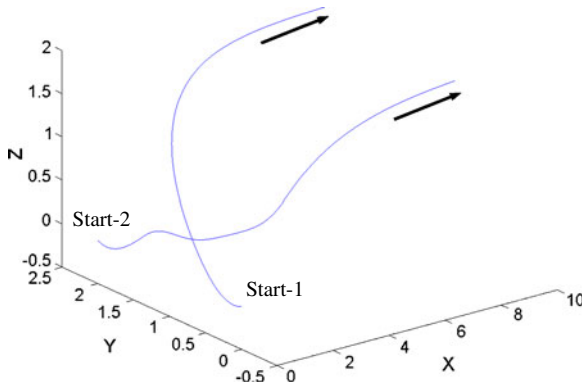


Fig. 21 Trajectories of the UAVs

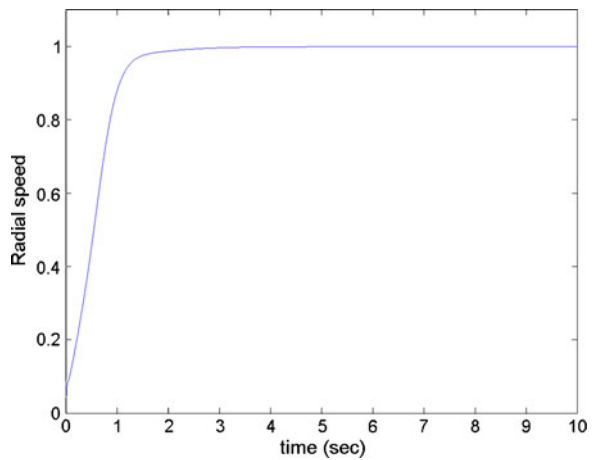


Fig. 23 Radial speed of the non-cooperative UAV

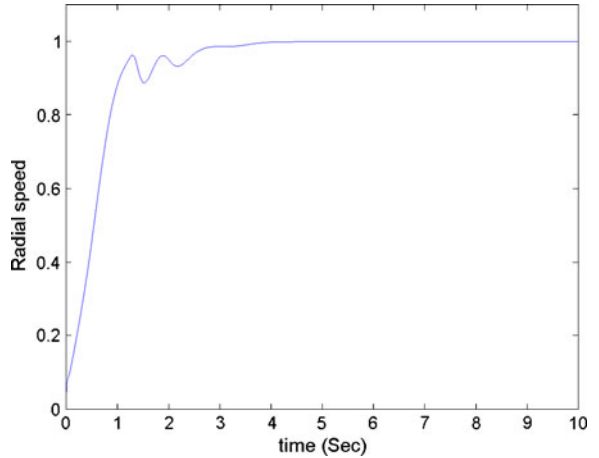


Fig. 24 Radial speed of the maneuvering UAV

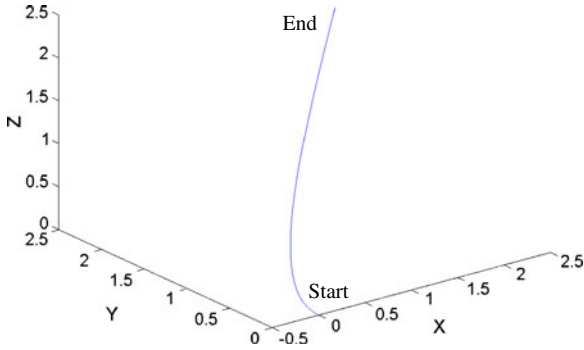


Fig. 25 Spatial trajectory

6.2 The Redundant Actuators Case

The ability of the controller to deal with high redundancy in the actuation is demonstrated using the following simulation example. A spherical system is used with six control inputs Eqs. 56 and 57. The parameters of the controller are: $K_\lambda = 1$, $K_u = 1$, $x(0) = y(0) = z(0) = 0$, $v(0) = 0$, $\theta(0) = \pi/2$, $\phi(0) = \pi/2$, $x_T = y_T = z_T = 2$. The radial speed of the system is required to be as close as possible to $v_r=1$. Figure 25 shows the 3-D spatial trajectory and Fig. 26 shows the corresponding xyz components. As can be seen the trajectory converged to the target in a well-behaved manner. It can also be seen that the en route radial velocity (Fig. 27) converge to the desired radial velocity. The local orientation angles are shown in Fig. 28. The six control signals are shown in Fig. 29. As can

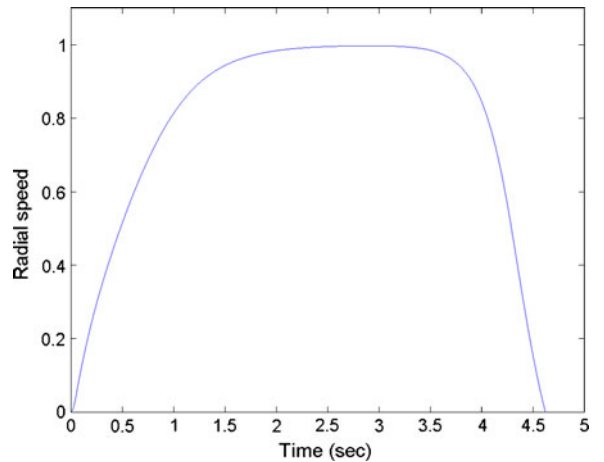


Fig. 27 Radial speed

be seen the signals are well-behaved.

$$\begin{aligned}\dot{x} &= v \cdot C\varphi C\theta \\ \dot{y} &= v \cdot S\varphi S\theta \\ \dot{z} &= v \cdot C\theta \\ \dot{v} &= u_1 + u_4 \\ \dot{\theta} &= u_2 + u_3 + u_5 \\ \dot{\phi} &= u_2 + u_4 + u_6\end{aligned}\quad (56)$$

$$\begin{aligned}J_\lambda &= \begin{bmatrix} C\varphi S\theta & -v \cdot S\varphi S\theta & v \cdot C\varphi C\theta \\ S\varphi S\theta & v \cdot C\varphi S\theta & v \cdot S\varphi C\theta \\ C\theta & \mathbf{0} & -v \cdot S\theta \end{bmatrix} \\ J_u &= \begin{bmatrix} 1 & 0 & 0 & 1 & 0 & 0 \\ 0 & 1 & 1 & 0 & 1 & 0 \\ 0 & 1 & 0 & 1 & 0 & 1 \end{bmatrix}\end{aligned}\quad (57)$$

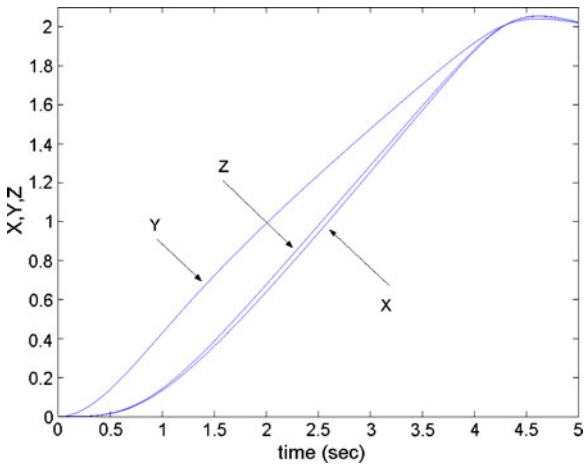


Fig. 26 x,y,z trajectory component

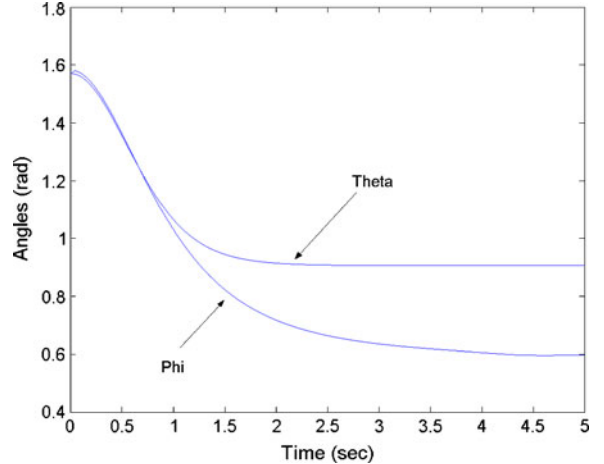


Fig. 28 Orientation angles

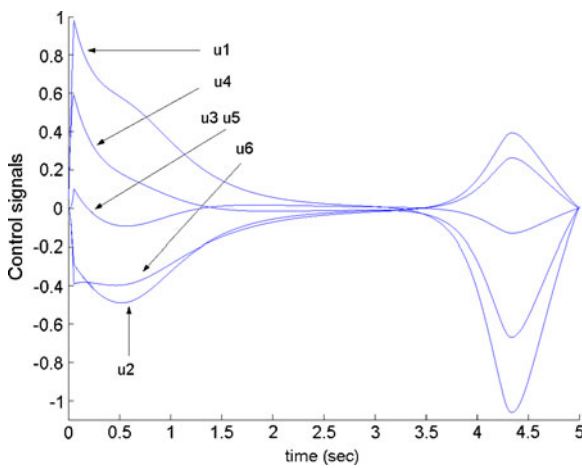


Fig. 29 Control inputs

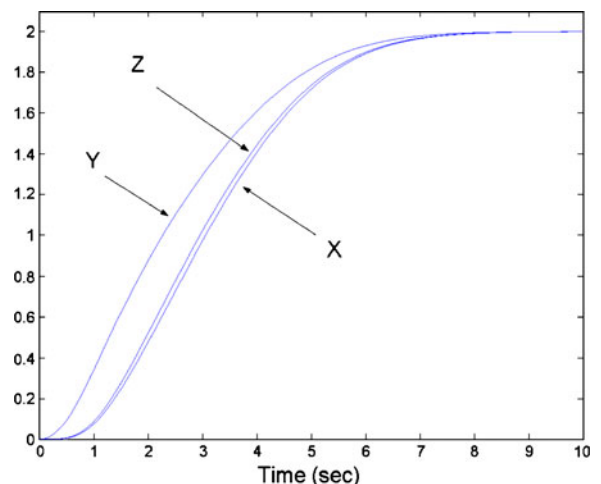


Fig. 31 X,Y,Z trajectory components—constrained

The same example in Fig. 25 is repeated with the absolute values of the control components constrained not to exceed 0.4. As can be seen from Figs. 30 and 31 the trajectory still converged to the target point in a well-behaved manner. The control components are shown in Fig. 32; they are well-behaved and strictly restricted to the desired region.

While for this case the constrained system converged to the same target point as the unconstrained system, the constrained control signal converged to a different value than the unconstrained signal. This is caused by the redundancy in the actuation and the fact that an infinite number of solutions for the actuation part in Eq. 56 could lead to zero motion of the local state at steady state (Fig. 33).

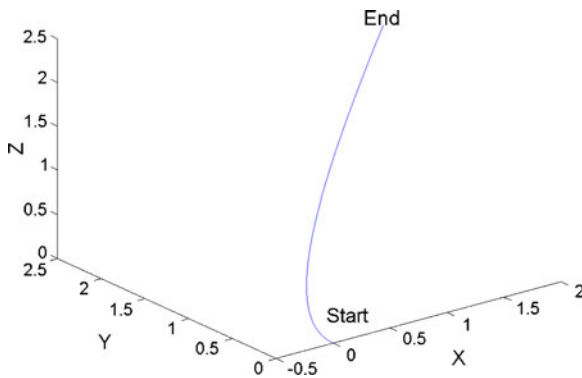


Fig. 30 3D trajectory—constrained

Constraining the controller does not limit the ability of the spherical UAV to perform relatively involved maneuvers. In the following example the UAV described by Eq. 56 is required to climb up to a height of $z = 2$ and perform a spiral maneuver in the x-y plane typically used in search patterns. The magnitude of each control signal is required not exceed 0.4. Also a unity radial speed is required. As can be seen from the 3D trajectory and its projection onto the x-y and y-z planes (Fig. 34), the controller was able to make the UAV efficiently perform the maneuver while keeping the control signals (Fig. 35) bounded and

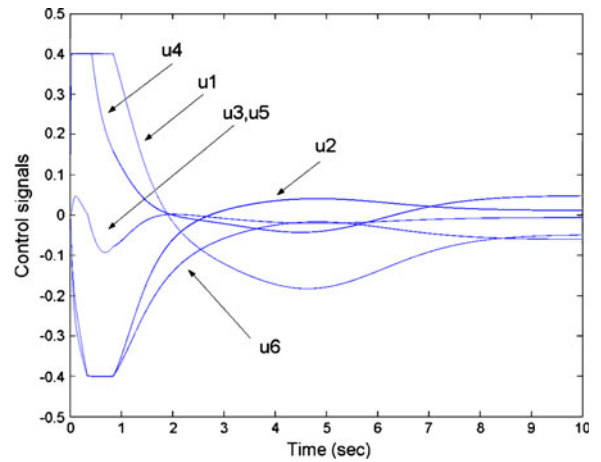


Fig. 32 Constrained control signals

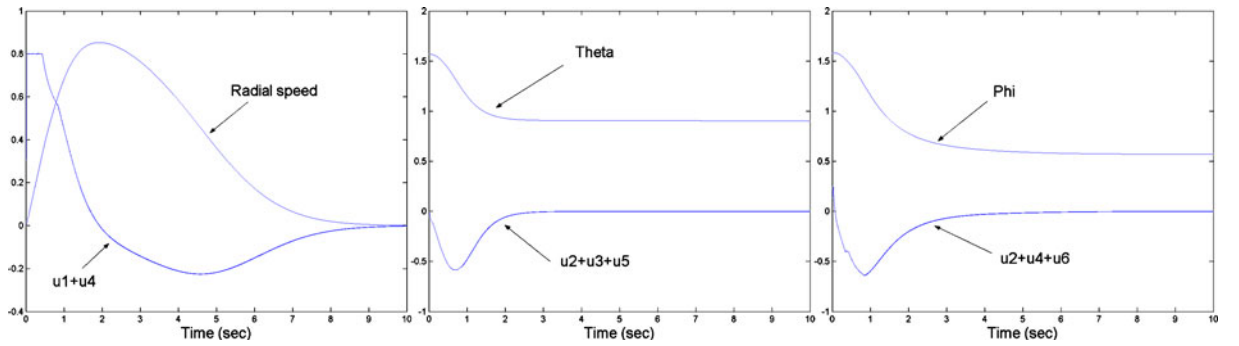


Fig. 33 Vanishing steady state actuation control—constrained system

well-behaved. The radial speed is well-behaved and settles on the desired value (Fig. 36). The local orientation angels (ϕ and θ) are also well-behaved (Fig. 37).

In the following example, the robustness of the control scheme is tested by adding noise to the control signals from the previous example. As can be seen, the trajectory remained well-behaved (Figs. 38 and 39). The noise effect on the radial velocity and the orientation is minimal (Figs. 40 and 41). The noisy control signal u_1 is shown in Fig. 42.

6.3 Dynamic and Kinematic Trajectories Compliance

This example demonstrates the ability of the suggested controller to make the dynamic trajectory comply with the kinematic one generated from a harmonic potential field planner. According to proposition-3, if the initial conditions are correctly set, it is possible to make the two trajectories identical hence enabling the dynamic system to en-

force all the constraints encoded in the kinematic path. The G-Harmonic potential method used to plan trajectories in ambiguous non-divisible environments [38, 39] is used to lay a kinematic path between two points in the X-Y projection of the UAV space. The X-Y environment is described by an intensity map where high intensity implies good fitness for motion to pass through while low intensity (dark regions) implies low fitness. The suggested controller is required to fly the redundant, spherical system (Eq. 56) in 3D space at an altitude $Z = 2$ using the XY information from the G-harmonic potential to move the UAV in the X-Y plane from the start point to the target. The magnitude of the control components is required not to exceed 0.4 and the reference radial velocity is 1. The initial values of the local UAV variables are: $v(0) = 0$, $\theta(0) = \phi(0) = \pi/4$. The controller was able to successfully drive the UAV to its target. Figure 43 shows the 3D trajectory and Fig. 44 shows the trajectory projection on the X-Z plane.

Figure 45 shows the projection of the trajectory in the X-Y plane superimposed on the environ-

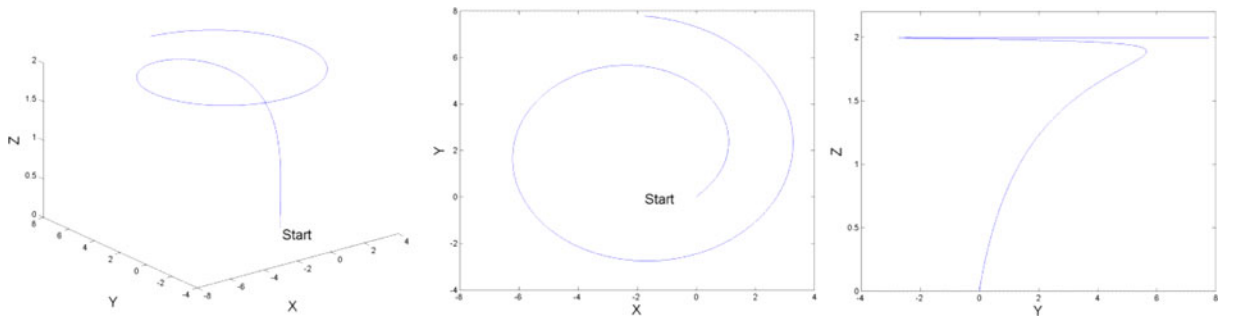


Fig. 34 The UAV 3D trajectory and its projection onto the X-Y and Y-Z planes

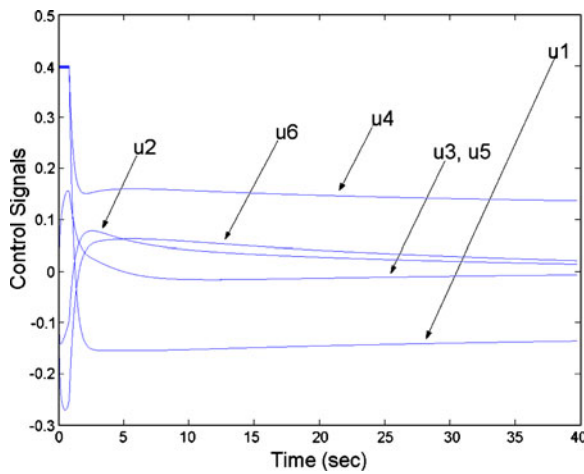


Fig. 35 The constrained control signals

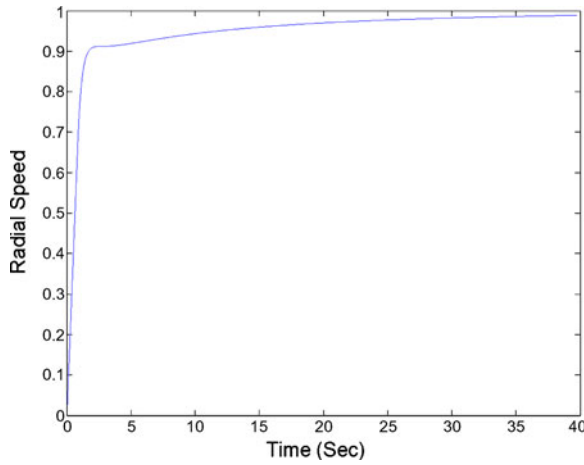


Fig. 36 The radial speed of the UAV

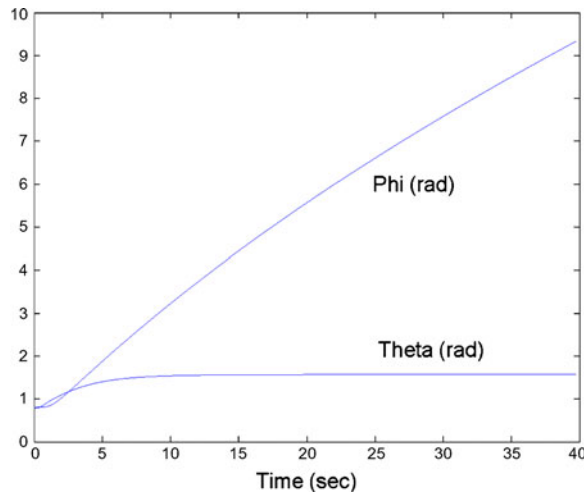


Fig. 37 The orientation angles of the UAV

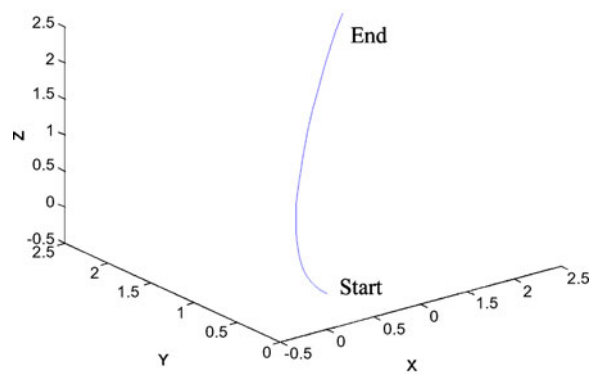


Fig. 38 Noisy spatial trajectory

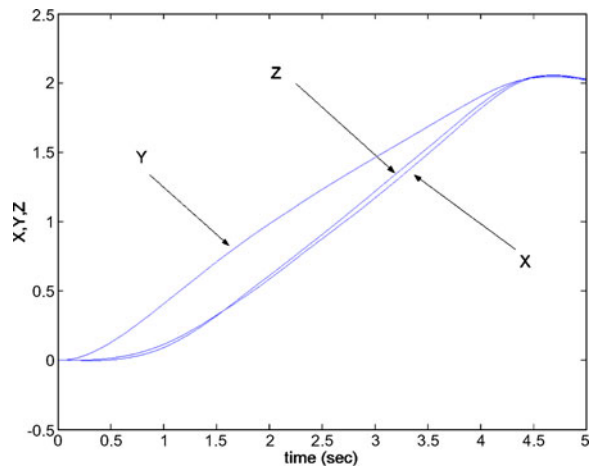


Fig. 39 Noisy x,y,z components

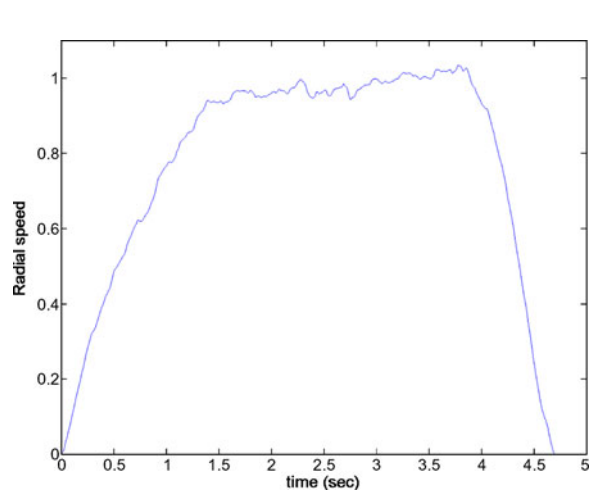


Fig. 40 Noisy radial speed

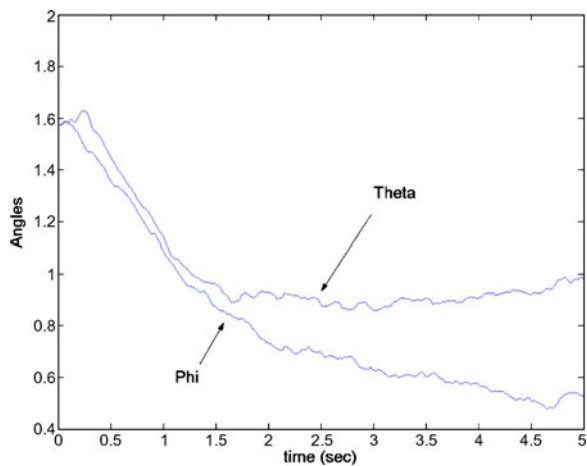


Fig. 41 Noisy orientation angles

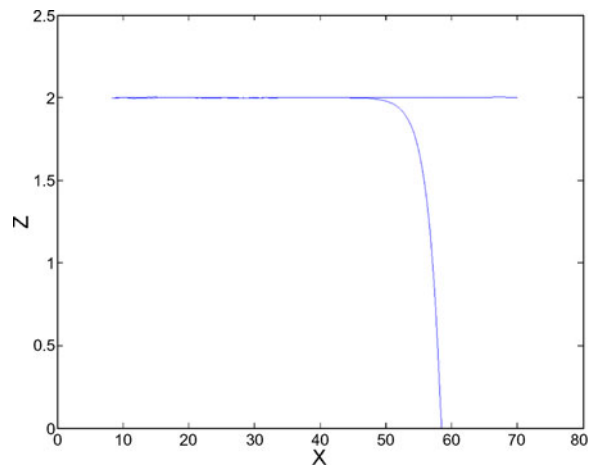


Fig. 44 X-Z trajectory projection

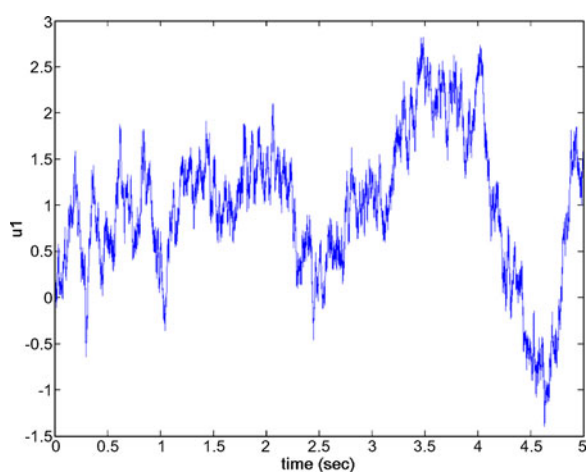


Fig. 42 Noisy u_1 control signal

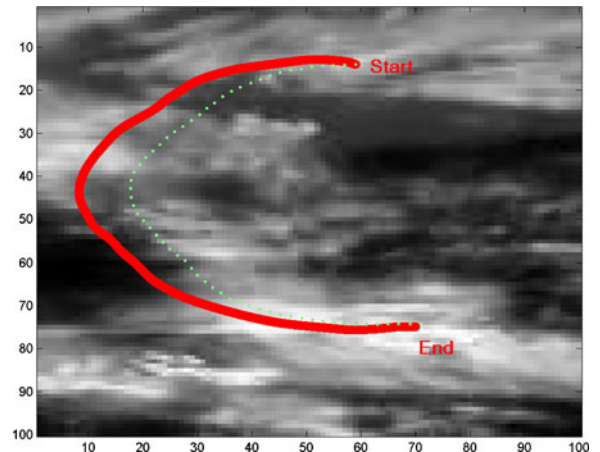


Fig. 45 Dynamic path deviating from the kinematic one

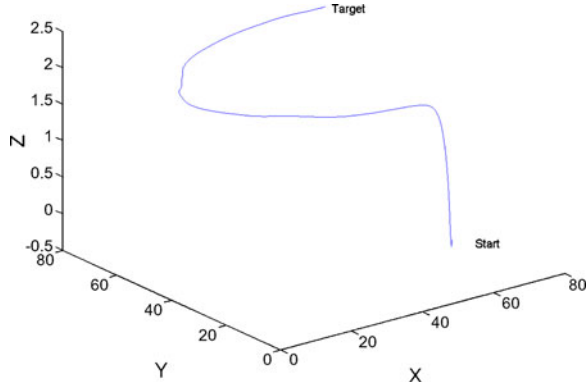


Fig. 43 3D trajectory

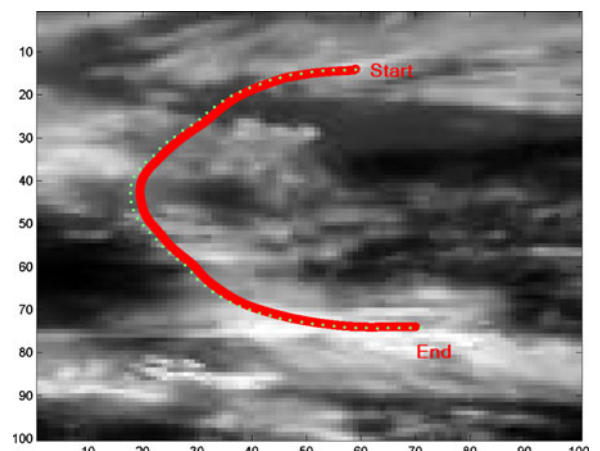


Fig. 46 Dynamic path close to kinematic path

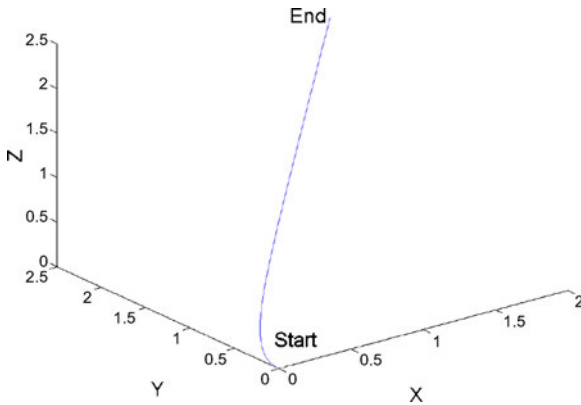


Fig. 47 Trajectory, underactuated UAV

ment. The solid line represents the dynamic trajectory and the dotted line represents the kinematic trajectory. As can be seen there is discrepancy between the two. In Fig. 46, the initial values of the local UAV variables are changed to $v(0) = 0$, $\theta(0) = \pi/4$, $\phi(0) = -0.225\pi$ to make the initial start of the two paths as much close as possible. As can be seen the kinematic and dynamic trajectories become almost identical.

6.4 The Underactuated Case

The following example examines the behavior of the controller for the under-actuated system described by Eqs. 58 and 59. The number of control variables in the previous systems are reduced to

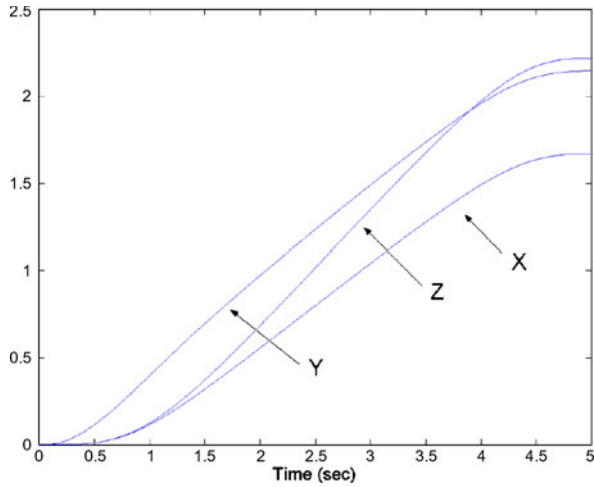


Fig. 48 XYZ components, underactuated UAV

only two which is less than the minimum needed to fully control the system in 3D space. The initial conditions, target and settings are the same as in the example shown in Fig. 25. As can be seen from Figs. 47 and 48 the system remained stable; however, it got trapped in a local minima failing to converge to the target.

$$\begin{aligned}\dot{x} &= v \cdot C\varphi C\theta \\ \dot{y} &= v \cdot S\varphi S\theta \\ \dot{z} &= v \cdot C\theta \\ \dot{v} &= u_1 \\ \dot{\theta} &= u_2 \\ \dot{\varphi} &= u_2\end{aligned}\quad (58)$$

$$\begin{aligned}J_\lambda &= \begin{bmatrix} C\varphi S\theta & -v \cdot S\varphi S\theta & v \cdot C\varphi C\theta \\ S\varphi S\theta & v \cdot C\varphi S\theta & v \cdot S\varphi C\theta \\ C\theta & 0 & -v \cdot S\theta \end{bmatrix} \\ J_u &= \begin{bmatrix} 1 & 0 \\ 0 & 1 \\ 0 & 1 \end{bmatrix}\end{aligned}\quad (59)$$

7 Conclusions

This paper demonstrates the ability of the harmonic potential field motion planning approach to deal with realistic planning problems such as the kinodynamic planning of motion for a UAV. Although the suggested solution is relatively simple (compared to the existing approaches) it amasses several important features desired for planning motion for a UAV. The structure of the controller is simple, making it highly possible to implement using inexpensive hardware. Despite this simplicity, the controller can tackle the exact model of a wide class of UAVs and provide an unconditionally stable, easy to tune response. The ability to effectively migrate, in a provably-correct manner, the kinematic path characteristics from an HPF-based planner to the dynamic trajectory of a UAV makes it possible to impose a wide class of constraints that accommodate the demands that a realistic environment imposes. It is worth noting that the manner in which the controller is constructed has the potential to tackle the full nonlinear model of a UAV with the rudder and aileron systems included [48, pp. 103]. The work in this paper clearly demonstrates the promising

potential the HPF approach has and its applicability to real situations.

Acknowledgements The author acknowledges the assistance of King Fahad University of Petroleum and Minerals in supporting this work.

References

1. Jones, C.: Unmanned aerial vehicles (UAVS) an assessment of historical operations and future possibilities. In: Paper presented to the research department air command and staff college in partial fulfillment of the graduation requirements of ACSC USAF, AU/ACSC/0230D/97-03 (1997)
2. Quaritsch, M., Kruggl, K., Wischounig-Strucl, D., Bhattacharya, S., Shah, M., Rinner, B.: Networked UAVs as aerial sensor network for disaster management applications. *Elektrotechnik & Informationstechnik* **127**(2), 56–63 (2010)
3. Lomax, A.S., Corso, W., Etro, J.F.: Employing unmanned aerial vehicles (UAVs) as an element of the integrated ocean observing system, OCEANS. In: Proceedings of MTS/IEEE, vol. 1, pp. 184–190 (2005)
4. Chen, H., Wang, X., Li, Y.: A survey of autonomous control for UAV. In: International Conf. on Artificial Intelligence and Computational Intelligence, pp. 267–271. Las Vegas, USA, 13–16 July 2009
5. Goerzen, C., Kong, Z., Mettler, B.: A survey of motion planning algorithms from the perspective of autonomous UAV guidance. *J. Intell. Robot. Syst.* **57**, 65–100 (2010)
6. Chao, H., Cao, Y., Chen, Y.: Autopilots for small unmanned aerial vehicles: a survey. *Int. J. Control. Autom. Syst.* **8**(1), 36–44 (2010)
7. Ren, W.: On constrained nonlinear tracking control of a small fixed-wing UAV. *J. Intell. Robot. Syst.* **48**(3), 525–537 (2007)
8. Roberts, P.J., Walker, R.A.: Fixed wing UAV navigation and control through integrated GNSS and vision. In: AIAA Guidance, Navigation, and Control Conference and Exhibit, pp. 1–13. San Francisco, California (2005)
9. Suresh, S., Kannan N.: Direct adaptive neural flight control system for an unstable unmanned aircraft. *Appl. Soft Comput.* **8**, 937–948 (2008)
10. Astrov, I., Pedai, A.: Control of hovering manoeuvres in unmanned helicopter for enhanced situational awareness. In: International Conference on Industrial Mechatronics and Automation, pp. 143–146 (2009)
11. Brown, A., Garcia, R.: Concepts and validation of a small-scale rotorcraft proportional integral derivative (PID) controller in a unique simulation environment. *J. Intell. Robot Syst.* **54**, 511–532 (2009)
12. Cai, G., Cai, A.K., Chen, B.M., Lee, T.H.: Construction, modeling and control of a mini autonomous UAV helicopter. In: Proceedings of the IEEE International Conference on Automation and Logistics Qingdao, pp. 449–454. China (2008)
13. Dierks, T., Jagannathan, S.: Output feedback control of a Quadrotor UAV using neural networks. *IEEE Trans. Neural Netw.* **21**(1), 50–66 (2010)
14. Kim, J., Kang, M., Park, S.: Accurate modeling and robust hovering control for a Quad-rotor VTOL aircraft. *J. Intell. Robot Syst.* **57**, 9–26 (2010)
15. Bouabdallah, S., Siegwart, R.: Full control of a Quadrotor. In: Proceedings of the 2007 IEEE/RSJ International Conference on Intelligent Robots and Systems San Diego, pp. 153–158. CA, USA (2007)
16. Lee, J., Min, B., Kim, E.: Autopilot design of tilt-rotor UAV using particle swarm optimization method. In: International Conference on Control, Automation and Systems, pp. 1629–1633. COEX, Seoul, Korea, 17–20 Oct 2007
17. Yanguo, S., Huanjin, W.: Design of flight control system for a small unmanned tilt rotor aircraft. *Chin. J. Aeronauti.* **22**, 250–256 (2009)
18. Escareno, J., Sanchez, A., Garcia, O., Lozano, R.: Triple tilting rotor mini-UAV: modeling and embedded control of the attitude. In: American Control Conference Westin Seattle Hotel, pp. 3476–3481. Seattle (2008)
19. Liu, Y., Pan, Z., Stirling, D., Naghdy, F.: Control of autonomous airship. In: Proceedings of the 2009 IEEE International Conference on Robotics and Biomimetics, pp. 2457–2462. Guilin, China (2009)
20. Knoebel, N.B., McLain, T.W.: Adaptive quaternion control of a miniature tailsitter UAV. In: American Control Conference Westin Seattle Hotel, pp. 2340–2345. Seattle, Washington, USA, 11–13 June 2008
21. Watanabe, M., Ochi, Y.: Modeling and motion analysis for a powered paraglider (PPG). SICE, 2007, pp. 3007–3012. Kagawa University, Japan (2007)
22. Leven, S., Zufferey J., Floreano D.: A minimalist control strategy for small UAVs. In: The 2009 IEEE/RSJ International Conference on Intelligent Robots and Systems, pp. 2873–2878. St. Louis, USA (2009)
23. Xu, Y.: Nonlinear robust stochastic control for unmanned aerial vehicles. In: 2009 American Control Conference Hyatt Regency Riverfront, pp. 2819–2824. St. Louis, MO, USA (2009)
24. Shehab, S., Rodrigues, L.: Preliminary results on UAV path following using piecewise-affine control. In: Proceedings of the 2005 IEEE Conference on Control Applications, pp. 358–363. Toronto, Canada (2005)
25. Kakirde, N.P., Davari, A., Wang, J.: Trajectory tracking of unmanned aerial vehicle using servomechanism strategy. In: Proceedings of the Thirty-Seventh South-eastern Symposium on System Theory, SSST ‘05, pp. 163–166, 20–22 Mar 2005
26. Lei, X., Liang, J., Wang, S., Wang, T.: An integrated navigation system for a small UAV using low-cost sensors. In: Proceedings of the 2008 IEEE International Conference on Information and Automation Zhangjiajie, pp. 765–769. China, 20–23 June 2008
27. McInnes, C.: Velocity field path-planning for single and multiple unmanned aerial vehicles. *Aeronaut. J.* **107**(1073), 419–426 (2003)

-
28. Yang, K., Gan, S., Sukkarieh, S.: An efficient path planning and control algorithm for RUAU's in unknown and cluttered environments. *J. Intell. Robot. Syst.* **57**, 101–122 (2010)
29. Jun, J., Pei-bei, M., Dan, L., Xiao-jie, Z.: Time control based on three-dimensional dynamic path planning. In: Proceedings of the IEEE International Conference on Automation and Logistics Shenyang, pp. 1832–1837. China (2009)
30. Yu, J., Xu, Q., Zhao, G., Zhang, R.: A scheme of integrated guidance/autopilot design for UAV based on TSM control. In: 2007 IEEE International Conference on Control and Automation WeDP-4 Guangzhou, pp. 707–711. China (2007)
31. Pastor, E., Royo, J.: A hardware/software architecture for UAV payload and mission control. In: 25th Digital Avionics Systems Conference, IEEE/AIAA, pp. 5B4-1–5B4-8, 15–19 Oct 2006
32. Hameed, T., Zhang, W.: Conceptual designing—unmanned aerial vehicle flight control system. In: The 9th International Conference on Electronic Measurement & Instruments (ICEMI) will be held on 16–18 August, vol. 3, Beijing, China, pp. 712–716 (2009)
33. Connolly, C., Weiss, R., Burns, J.: Path planning using laplace equation. In: IEEE Int. Conf. Robotics Automat., Cincinnati, OH, pp. 2102–2106 (1990)
34. Akashita, S., Kawamura, S., Hayashi, K.: New navigation function utilizing hydrodynamic potential for mobile robots. In: IEEE Int. Workshop Intelli. Motion Contr., Istanbul, Turkey, pp. 413–417 (1990)
35. Khatib, O.: Real-time obstacle avoidance for manipulators and mobile robots. In: IEEE Int. Conf. Robotics and Automation, St. Louis, MO, pp. 500–505 (1985)
36. Masoud, A.: An informationally-open, organizationally-closed control structure for navigating a robot in an unknown, stationary environment. In: 2003 IEEE International Symposium on Intelligent Control, Houston, Texas, USA, pp. 614–619 (2003)
37. Masoud, S., Masoud, A.: Motion planning in the presence of directional and obstacle avoidance constraints using nonlinear anisotropic, harmonic potential fields: a physical metaphor. *IEEE Trans. Syst. Man Cybern., Part A, Syst. Humans* **32**(6), 705–723 (2002)
38. Masoud, A.: A harmonic potential field approach with a probabilistic space descriptor for planning in non-divisible environments. In: IEEE International Conference on Robotics and Automation, Kobe, Japan, pp. 3774–3779, 12–17 May 2009
39. Masoud, A.: Planning with gamma-harmonic functions. In: 2010 IEEE/ASME International Conference on Advanced Intelligent Mechatronics, Montreal, Canada, 6–9 July 2010
40. Gupta, R., Masoud, A., Chow, M.: A network based, delay-tolerant, integrated navigation system for a differential drive UGV using harmonic potential field. In: Proceedings of the 45th IEEE Conference on Decision & Control Manchester Grand Hyatt Hotel, San Diego, CA, USA, pp. 1870–1875, 13–15 Dec 2006
41. Masoud, S., Masoud, A.: Constrained motion control using vector potential fields. *IEEE Trans. Syst. Man Cybern., Part A, Syst. Humans* **30**(2), 251–272 (2000)
42. Masoud, A.: Kinodynamic motion planning: a novel type of nonlinear, passive damping forces and advantages. *IEEE Robot. Autom. Mag.* **17**(1), 85–99 (2010)
43. Masoud, A.: A harmonic potential field approach for navigating a rigid, nonholonomic robot in a cluttered environment. In: IEEE International Conference on Robotics and Automation, Kobe, Japan, pp. 3993–3999 (2009)
44. Joshi, V.A., Banavar, R.N.: Motion analysis of a spherical mobile robot. *Robotica* **27**, 343–353. Cambridge University Press (2009)
45. Nahon, M.: A simplified dynamics model for autonomous underwater vehicles. In: Proc 1996 Symp. on Autonomous Underwater Vehicle Technology, New York, pp. 373–379 (1996)
46. Vinh, N.: Flight Mechanics of High-Performance Aircraft. Cambridge University Press (1995)
47. Masoud, A.: Decentralized, self-organizing, potential field-based control for individually-motivated, mobile agents in a cluttered environment: a vector-harmonic potential field approach. *IEEE Trans. Syst. Man Cybern., Part A, Syst. Humans* **37**(2), 372–390 (2007)
48. Etkin, E.: Dynamics of Flight, 2nd edn. Wiley, New York (1982)
49. LaSalle, J.: Some extensions of Lyapunov's second method. *IRE Trans. Circuit Theory* **CT-7**(3), 520–527 (1960)
50. Masoud, A.: A virtual velocity attractor, harmonic potential approach for joint planning and control of a UAV. In: American Control Conference 2011, San Francesco, 29 June–1 July 2011